demanding that it vanish at $z=1$ and compare the expression (d) with (24), we get

$$C_1=A_1(c/b)^{\frac{1}{4}+\frac{1}{2}\mu}D_1, \quad \text{(i)}$$

$$C_2=A_2(b/c)^{-\frac{1}{4}+\frac{1}{2}\mu}D_2+A_3(b/c)^{\mu}C_1. \quad \text{(j)}$$

Here A_1, A_2, A_3 are numbers. These equations show that as D_1, D_3, D_4 vary over their range and D_2 is zero, C_1, C_3, C_4 do likewise, while C_2 takes a finite value linked to C_1. However for small ϵ, that is small b/c, this value is very much smaller than C_1 which itself is limited by the size of the reaction zone. Now as D_2 passes through its finite range allowed by (f), C_2 varies independently of C_1 within a small range; this range is given by

$$\Delta C_2=A_2(b/c)^{\frac{1}{2}\mu-\frac{1}{4}}(D_{\min}+D_{\max}), \quad \text{(k)}$$

and hence

$$\Delta C_2 \propto \epsilon^{\frac{1}{2}\mu-\frac{1}{4}}. \quad \text{(l)}$$

The relation (k) is equivalent to (32), and (l) to (33); thus the simple reasoning yielding (33) is justified.

PHYSICAL REVIEW VOLUME 90, NUMBER 5 JUNE 1, 1953

The Stopping of Heavy Ions in Gases

G. E. Evans, P. M. Stier, and C. F. Barnett
Oak Ridge National Laboratory, Oak Ridge, Tennessee

(Received October 6, 1952)

The extrapolated ionization range for the ions He^+, N^+, Ne^+, and A^+ in the stopping gases He, N_2, air, and A has been determined as a function of energy in the energy range from *ca* 20 kev to *ca* 250 kev, using monoenergetic heavy ions produced in a Cockcroft-Walton accelerator. A collimated beam of heavy ions is admitted to the range chamber via a three-stage differential pumping system so as to avoid the use of foil windows. The range was determined using a parallel plate ionization chamber mounted so as to permit translation parallel to the axis of the beam. It has been found that the range as measured at a pressure P is not inversely proportional to P, and an interpretation of this pressure effect has been given in terms of large angle scattering of the ions into regions outside of the volume swept out by the ionization chamber. A method of correcting for this pressure effect has been developed and applied to the data to yield range-energy curves which are independent of the ionization chamber size. The space distribution of ionization produced in a gas by a collimated beam of heavy ions has been determined for the same combinations of incident ion, stopping gas, and energy as above. The attenuation of the beam of ions is found to be approximately exponential in the axial direction and approximately Gaussian in the lateral direction. A method has been developed for computing the shape and size of a given ionization density contour at a given pressure if it is known at another pressure and the same energy.

I. INTRODUCTION

THE problem of determining the rate and mechanism of energy loss of high energy charged particles in matter has received a large amount of attention, both experimentally and theoretically, during the past few decades. The range, specific ionization, scattering, and straggling of protons, deuterons, and alpha-particles have been determined over wide energy intervals by various investigators and comprehensive summary reports have been published.[1] The theory of the mechanism of energy loss by these light particles is sufficiently well understood to allow a quantitative description of the processes of elastic and inelastic scattering in terms of simple classical or quantum-mechanical models, and the criteria for the validity of the models have been determined.[2] A much smaller amount of experimental work has been done on the range and specific ionization of fission fragments, yet even in this much more complex problem, qualitative agreement between theory and experiment has been achieved.[3]

In almost all of the research done in this field in the past, the velocity of the incident ion has been large compared to the velocity of its outermost electrons. Furthermore, in a majority of the previous research, the mass of the incident ion has been small compared to the atomic mass of the stopping material. There remains a large and practically unexplored field of penetration phenomena in which the velocity of the ion is of the same order of magnitude or smaller than the velocity of its outermost electrons, and in which the mass of the incident ion is allowed to vary over wide limits. Work within this latter field has been limited because of the major difficulties in theoretical interpretation of results[4] and because the experimental

[1] H. A. Bethe, Atomic Energy Commission Report AECU 347 (BNL-T-7); Aron, Hoffman, and Williams, Atomic Energy Commission Report AECU 103 (UCRL 121 rev, 2nd ed.) (unpublished).

[2] See, e.g., H. A. Bethe, Revs. Modern Phys. **22**, 213 (1950); M. S. Livingston and H. A. Bethe, Revs. Modern Phys. **9**, 245 (1937); E. J. Williams, Revs. Modern Phys. **17**, 217 (1945).

[3] Katcoff, Miskel, and Stanley, Phys. Rev. **74**, 631 (1948); N. O. Lassen, Kgl. Danske Videnskab. Selskab, Mat.-fys. Medd. **25**, No. 11 (1949).

[4] N. Bohr, Kgl. Danske Videnskab. Selskab, Mat.-fys. Medd. **18**, No. 8 (1948).

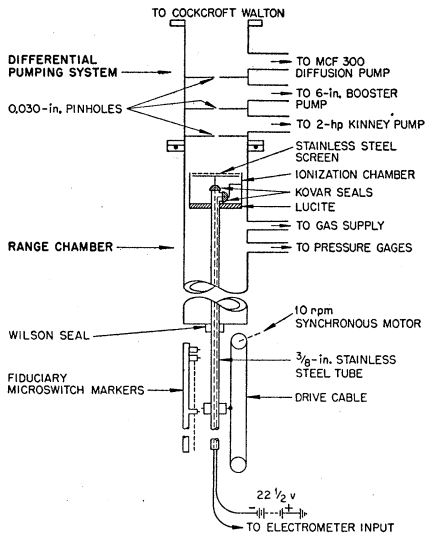

FIG. 1. Differential pumping system and range chamber.

techniques which have been developed in the study of high energy charged particles do not apply to this lower energy region. (In particular, foils cannot be used as windows to separate various portions of the path of such particles because of their very short range in solids, and pulses produced in counters are too small to allow accurate differential pulse height analysis.)

The almost complete lack of either experimental or theoretical information as to the behavior of charged particles in this energy region does not imply that this information is of little significance. The recoil particles produced by bombardment of materials with high energy charged particles or with fast neutrons fall within this energy range, and it is to these recoil particles that the effects known as "radiation damage" are in part ascribed. While a large percentage of the total ionization produced by high energy radiation occurs within an energy region where theoretical interpretation is possible, a majority of the lattice displacements in solid stopping materials occur for particle energies so low that neither classical nor quantum-mechanical interpretations have achieved more than order-of-magnitude success.[5]

This paper is the first report of an experimental program of study of the properties of low energy heavy ions.[6] The masses of the ions which are being studied vary from 1 to 40 atomic mass units, including hydrogen, helium, nitrogen, neon, and argon, and the energy of the ions is variable from a few kev to several hundred kev. Various stopping gases are employed, including helium, nitrogen, air, and argon. The properties which are being investigated include range-energy relationship, specific ionization, W (electron volts per ion pair), stopping power (dE/dx), range straggling, elastic scattering, and electron capture-loss phenomena. Reported in this paper are the results of experiments on the range-energy relation and on the space distribution of ionization produced by heavy ions.

[5] F. Seitz, Disc. Faraday Soc. (No. 5) 271 (1949).

[6] Oak Ridge National Laboratory, Physics Division, Unclassified Quarterly Reports: ORNL 1289, ORNL 1278, ORNL 1164 (unpublished).

II. PRODUCTION OF THE ION BEAM

Ions for use in these experiments were produced in a Phillips Ionization Gauge type source and accelerated in a conventional Cockcroft-Walton type accelerator. The accelerating voltage has been calibrated against known nuclear reactions and is accurate to within about 1 percent. The high voltage supply is very stable, varying less than 0.2 percent in voltage over a period of 15 minutes or more. The ion source, which will be described in more detail elsewhere,[7] is capable of producing heavy ion currents at the target position of 0.5 ma or higher and has operated stably for an operating life of more than 500 hours. The maximum fluctuations in ion source output current can be held to less than 1 percent over a period of 15 minutes or more. After passing through a magnetic mass analyzer, the beam of monoenergetic heavy ions enters the gas target assembly by means of the differential pumping system shown in Fig. 1.

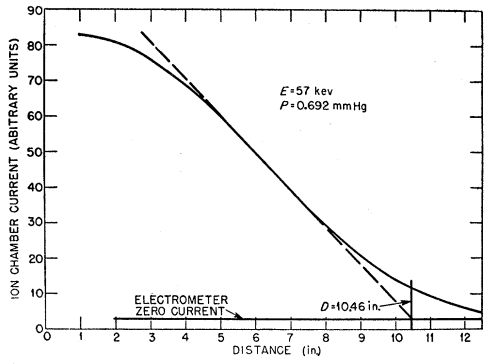

FIG. 2. Typical range-ionization curve for low energy heavy ions. (N^+ ions in air).

In addition to affording entrance of the ion beam from the vacuum of the accelerator tube into the 0.1–20-mm Hg pressure of the gas target without passing through solid foils, the differential pumping system pinholes serve as efficient collimators, producing a beam approximately 0.030 inch in diameter. The pressure drops by a factor of approximately 100:1 across each pinhole of the system.

III. THE RANGE-ENERGY RELATION

The equipment used for the experimental determination of the ionization range is shown schematically in Fig. 1. A collimated beam of monoenergetic heavy ions enters the range chamber via the differential pumping system pinholes, and the ionization current

[7] Barnett, Stier, and Evans, Rev. Sci. Instr. (to be published).

produced in a parallel plate ionization chamber is measured using a balanced bridge electrometer.[8] Ions enter the ionization chamber through a high-transparency stainless steel grid maintained at 22 volts negative with respect to ground. The effective size of the ion chamber is 3 inches in diameter and 0.040 inch thick. This thickness is less than 1 percent of the smallest ranges measured (approximately 4 inches), and hence the recorded distance to the ionization chamber was measured relative to the geometrical center of the chamber. The stainless steel tube supporting the ion chamber slides in a Wilson seal and is attached to a synchronous motor drive to permit automatic recording of range curves. In order to reduce the number of runs which must be rejected because of a shift in operating conditions during the run, the speed of the drive motor was set as fast as was consistent with the speed of response of the electrometer and recorder. The electrometer output is recorded on a Speedomax recorder, and fiduciary marks are supplied by a system of microswitches attached to the ionization chamber

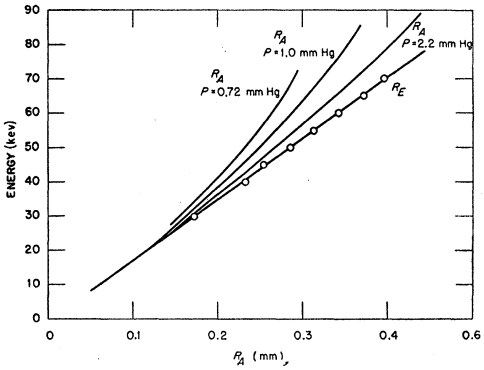

FIG. 3. Range-energy relation for N_2^+ in air at various pressures.

drive mechanism. The fiduciary marker system was machined to a tolerance of 0.005 inch, so that the measurement of axial distances should introduce a negligible error. The pressure of gas in the range chamber is measured by two McLeod gauges calibrated to 1 percent accuracy and checked against each other at least daily, and is continuously monitored by means of an Alphatron gauge. A typical range curve obtained with this equipment is shown in Fig. 2. Such curves obtained under operating conditions comparable except for changes in initial ion beam intensity by a factor of as much as 100 agree to within 2 percent, including subjective errors in selecting the straight line portion of the curve. It follows that within the range of initial ion beam intensities available, the extrapolated ionization range as measured is independent of the initial ion beam intensity. The data presented have been taken from the results of over 500 ionization current *versus* distance curves similar to Fig. 2.

[8] Employing a General Electric 5674 Electrometer tube; see J. M. Lafferty and K. H. Kingdom, J. Appl. Phys. **17**, 894 (1946).

From curves such as Fig. 2, values of the extrapolated ionization range at pressure P, (R_P), are obtained by extrapolating the linear portion of the curve to intersect the base line at zero electrometer current. From these values of R_P the computed range at NTP (20°C, 1 atmos) is determined by multiplying by $P/760$; the symbol R_A will be used for this range at NTP expressed in millimeters.

Values of R_A are shown as a function of energy E in Fig. 3 for N_2^+ stopping in air. It is evident that the value of R_A at a given energy is a function of the pressure at which the range was determined. Similar plots of R_A *vs* E for other incident ions and stopping gases demonstrate that this "pressure effect" is most pronounced for $M_1 = M_2$ and at low energies, where M_1 and M_2 are the atomic masses of incident ion and stopping gas respectively. These facts considered together with the geometry of the range chamber suggest that the pressure effect is due to elastic scattering of ions outside of the cylindrical volume swept out by the ionization chamber, so that at low pressures a smaller percentage of the total ionization is detected by the ionization chamber, particularly for large values of the axial distance R. As a result the apparent range R_A is smaller when measured at low pressures than when measured at higher pressures.[9] This pressure effect could be eliminated either by use of a very large ionization chamber so as to collect all of the scattered ions, or by

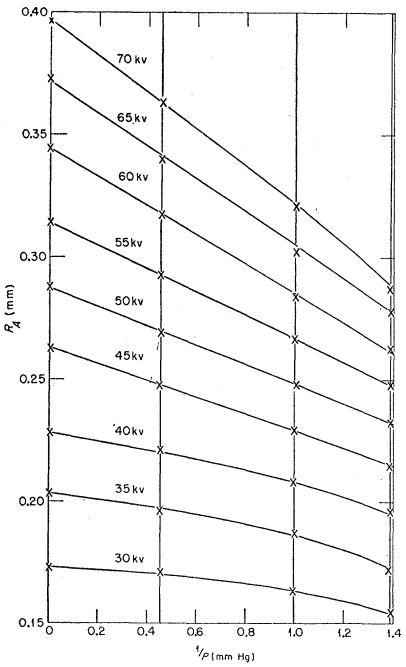

FIG. 4. Extrapolation of ionization range to high pressure.

[9] T. A. Jorgensen and co-workers (private communication) have described a similar effect in range determinations for low energy protons in various stopping gases and have independently reached a similar interpretation. In the Jorgensen experiments, the effective diameter of the ion chamber is variable, rather than the pressure.

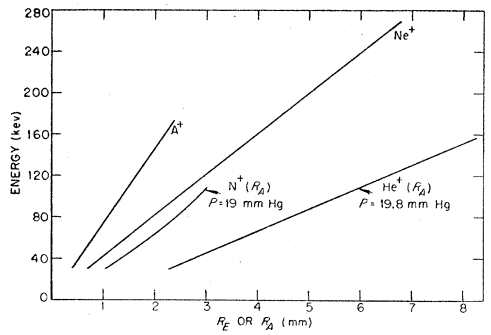

FIG. 5. Range of various ions in helium.

using a sufficiently high pressure to confine all of the scattered ions within the volume swept out by the ionization chamber. Since it was not found practical to meet these conditions experimentally, the effect of pressure upon the range was corrected for by plotting

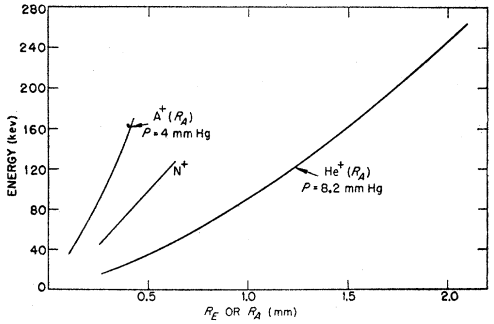

FIG. 6. Range of various ions in nitrogen.

the values of R_A obtained at various pressures against $1/P$ and extrapolating to $1/P=0$. Values of this corrected extrapolated ionization range R_E are shown in

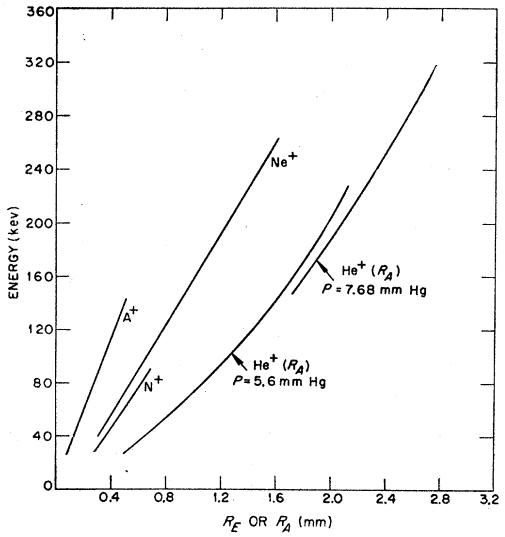

FIG. 7. Range of various ions in argon.

Fig. 3 and are seen to fall on a straight line within the errors of the experimental technique. A typical plot of R_A *versus* $1/P$, for the data from which Fig. 3 were drawn, is shown in Fig. 4. While a curvilinear extrapolation is well known to be highly dangerous as a source of indeterminate error, it is felt that the R_E *versus* E curves give a better representation of the ionization range-energy relation than do the uncorrected R_A *vs* E curves. Values of R_E or R_A as a function of E for various ions stopping in He, N_2, and A are shown in Figs. 5, 6, and 7. For those incident ion-stopping gas combinations where insufficient data were available to carry out the extrapolation against $1/P$ a typical curve of R_A *vs* E is shown, together with

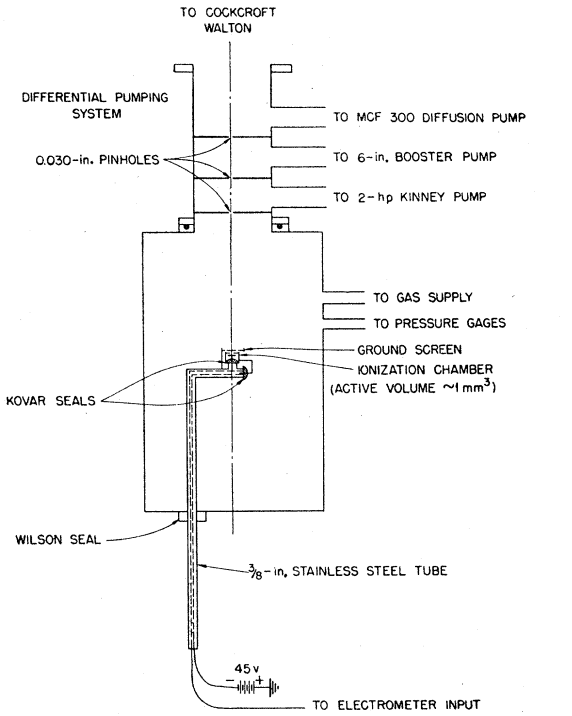

FIG. 8. Gas chamber for study of ionization distribution.

the pressure at which the experiment was performed. Most of the range-energy curves are nearly linear, and when extrapolated intersect the zero energy abscissa at positive range values. This implies that in this energy region the total stopping power is nearly constant, but will decrease at lower energies.

IV. SPACE DISTRIBUTION OF IONIZATION

The gas target shown attached to the differential pumping system in Fig. 8 was constructed to study the axial and lateral extent of the ionization produced when a collimated beam of ions enters a volume of gas. The small ionization chamber has an active volume of about 1 mm^3 and is mounted eccentrically on a rod sliding in a Wilson seal, so that by suitable rotation

and translation of the supporting rod the ionization chamber can be positioned at any representative axial or lateral position relative to the point of entry of the beam into the gas. The ionization chamber consists of two parallel plates, the lower serving as the electron collector and the upper containing a 0.06 of an inch diameter hole for entrance of ions. In normal use the upper perforated plate was maintained at a negative potential of about 45 volts. The ionization chamber is shielded with a grounded wire grid.

Typical plots of ionization density C *vs* location in space (R,r) are shown in Figs. 9–11. The ionization

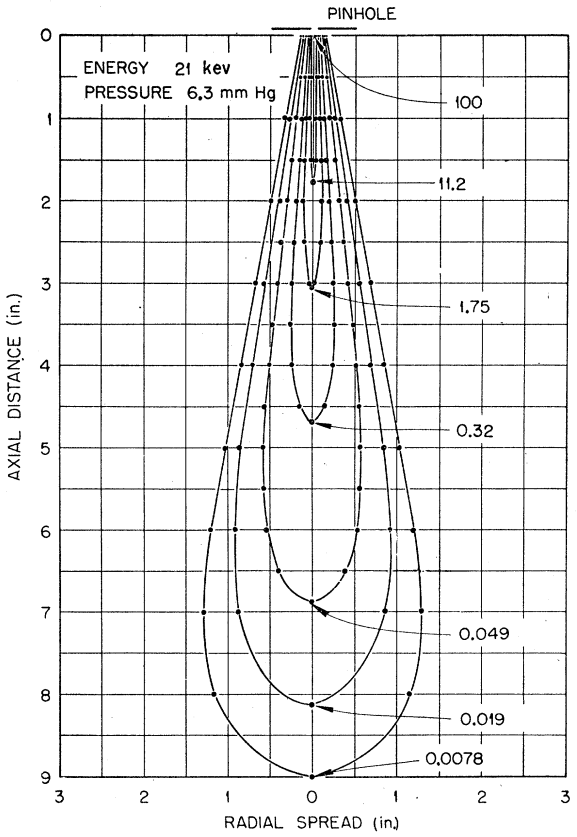

FIG. 9. Space distribution of ionization: He^+ ions in argon. The numbers shown adjacent to the various contours are the appropriate values of C.

density is here defined as the ionization current at (R,r) divided by the volume of the ionization chamber, multiplied by the ratio of a fixed reference current (100 units) to the ionization chamber current at the position (0,0); where R and r are the axial and lateral distances of a given point from the point of entry of the beam at (0,0). The values of r were determined for a given value of C by measuring the angle 2θ between the two positions of the ionization chamber (one on each side of the beam axis) for which the measured ionization density is C. The corresponding value of r is then directly obtained from the value of $\sin(\theta/2)$ from

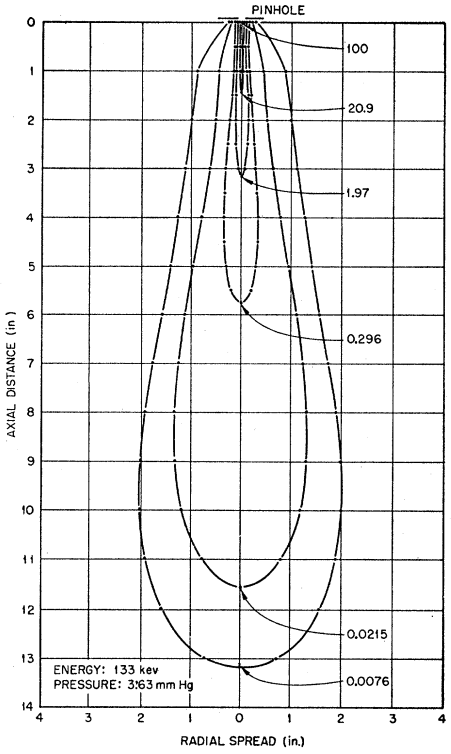

FIG. 10. Space distribution of ionization: A^+ ions in helium. The numbers shown adjacent to the various contours are the appropriate values of C.

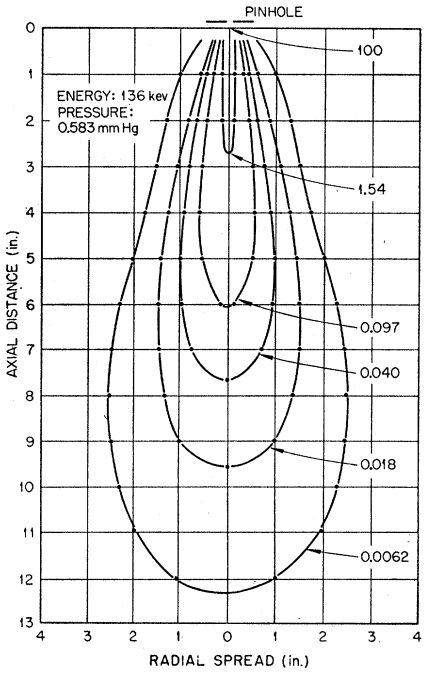

FIG. 11. Space distribution of ionization: A^+ ions in argon. The numbers shown adjacent to the various contours are the appropriate values of C.

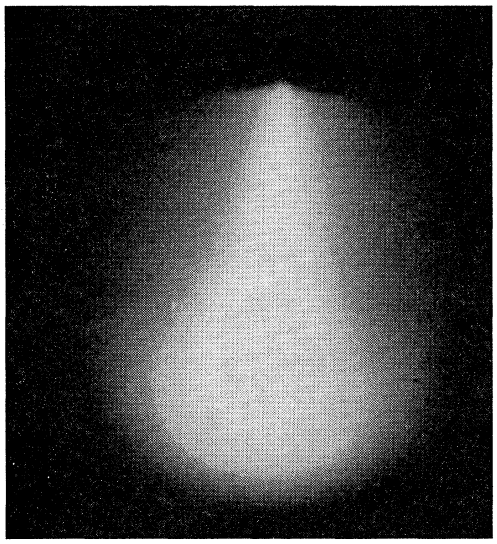

FIG. 12. Photograph of the luminescence produced by the beam: He^+ ions in argon. Energy = 136 kev.

the relation $r = 2d \sin(\theta/2)$ where d is the length of the eccentric arm supporting the ionization chamber. In Figs. 9. 10, and 11, the ionization density curves are shown reflected at the beam axis, assuming radial symmetry, in order to demonstrate the shape more directly. Similar systems of contour curves have been obtained for the other possible combinations of the incident ions He^+, Ne^+, N^+, and A^+ in the stopping gases He, N_2, and A at a variety of pressures and initial energies.

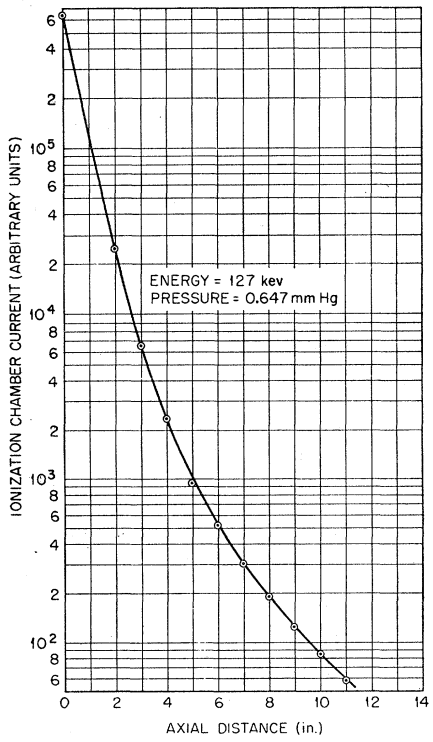

FIG. 13. Axial attenuation of ionization: A^+ ions in argon.

In Fig. 12 is shown a photograph of the beam (He^+ in A at 136 kev, $P = 26$-mm Hg) taken through a window in the side of the gas target assembly. The similarity of the luminous region in the gas and the contour plot of ionization density shown in Fig. 9 is evident.

In Fig. 13 is shown the variation of the ionization density along the axis of the beam, for argon ions stopping in argon gas, as measured with the small (1 mm^3) ionization chamber. An exponential attenuation along the axis of the beam could be explained in terms of elastic scattering of ions from the beam axis, which should follow an exponential law if the axial attenuation of ionization current measured by a very small ionization chamber is due primarily to loss of ions from the central beam rather than to reduction in the energy of ions in the central beam.

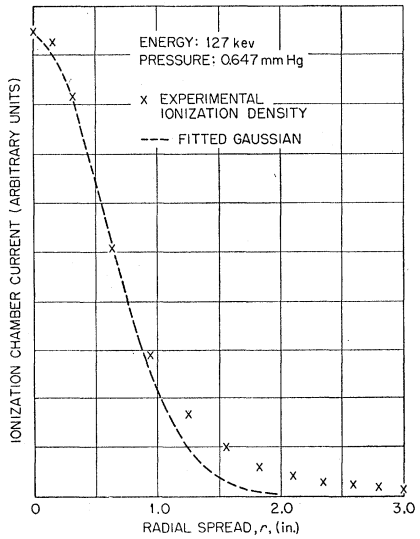

FIG. 14. Radial attenuation of ionization: A^+ ions in argon.

In Fig. 14 is shown the variation of the relative ionization along a line normal to the axis of the beam, 5 inches from the entrance pinhole. On the same graph is shown a Gaussian curve fitted to the experimental data at radial distances of zero and one inch. The experimental data are represented quite well by a Gaussian curve for small values of r, but for large values of r the ionization density is greater than that corresponding to a Gaussian distribution.

By combining the results shown in Figs. 13 and 14, it is possible to represent the over-all distribution of ionization in space by an empirical formula of the type $C = \exp(-AR - Br^2/R^2)$. Since the axial attenuation is not strictly exponential and the radial attenuation is not strictly Gaussian, it is evident that the product above will combine the errors of both approximations.

Figure 15 shows one ionization density contour for argon ions in argon gas at 136 kev, $P=0.38$-mm Hg fitted by the function $C=\exp(-0.37R-83.5r^2/R^2)$.

In the experimental determination of ionization density contour shapes, it has been found necessary to adjust the pressure so as to obtain contours whose physical size falls within fairly well defined limits. Contours which are too large suffer interference from the walls of the scattering chamber, while contours which are too small do not permit accurate measurement of distances. It has not been found possible to select a single scattering chamber pressure which gives satisfactory experimental results for the wide range of parameters (M_1, M_2, and E) available. Hence, it is necessary to determine the manner in which the shape and size of a given contour varies with pressure in order to present results under standardized conditions. It is not possible to compute the shift in the location of a given ionization contour upon change in pressure simply by multiplying by the pressure ratio, for several reasons. The ionization chamber is open to the gas in the scattering chamber, and thus a change in gas pressure changes the response characteristics of the ionization chamber; and while a given ionization density contour decreases in size upon increase in pressure, the ionization chamber remains constant in size and thus intercepts a larger fraction of the total ionization volume. For positions (R,r) where the value of C changes slowly and uniformly with respect to both R and r (dC/dR and dC/dr both small and constant) the ionization current should be nearly proportional to the volume of the ionization chamber. This condition is obviously not satisfied for positions too close to (0,0). At the point (0,0) itself, for example, the ionization chamber current is nearly independent of ionization chamber diameter (provided only that this diameter is larger than the diameter of the entrance pinhole as was the case in these experiments) and varies as the ionization chamber thickness.

The considerations may be illustrated more quantitatively as follows: Assume that a small ionization chamber is placed at the position (R_1,r_1) in a gas at pressure P_1, and that the ionization chamber current is i_1'. If the ionization chamber current at the position (0,0) is i_1, then by definition $C_1=100i_1'/i_1$, where the volume of the ionization chamber is set equal to unity. If now the pressure is changed to P_2 and the ionization chamber is moved to the position (R_2,r_2) where $R_2=P_1R_1/P_2$ and $r_2=P_1r_1/P_2$, a different ionization i_2' will be read, and the value of the ionization current at the position (0,0) will now be a different value i_2. Define $C_2=100i_2'/i_2$. From the preceding discussion, it follows that for a constant initial ion beam,

$i_1/i_2=P_1/P_2$ and $i_1'/i_2'=P_1^3/P_2^3$. Hence $C_1/P_1^2=C_2/P_2^2$.

Thus upon changing the pressure from P_1 to P_2 and the ionization chamber position from (R_1,r_1) to $(P_1R_1/P_2, P_1r_1/P_2)$ the new value of the ionization density will be $C_2=C_1P_2^2/P_1^2$. It follows further that if V_1 is the volume in space enclosed by the contour C_1 and V_2 is the volume enclosed by the contour C_2 that $V_1/V_2=P_2^3/P_1^3=P_2C_2/P_1C_1$ and thus $C_2/C_1=P_1V_1/P_2V_2$. From these relationships it is seen that contours with the same value of C contain equal numbers of atoms, for the same incident ion, stopping gas, and initial energy. The relationships derived above have been checked experimentally for the systems He^+ in A, A^+ in He, He^+ in He, and A^+ in A with an observed error of about 5 percent in the relation $C_2=C_1P_2^2/P_1^2$ and a maximum error of less than 5 percent in the relation $C_2/C_1=P_1V_1/P_2V_2$. Predicted values of the ionization density

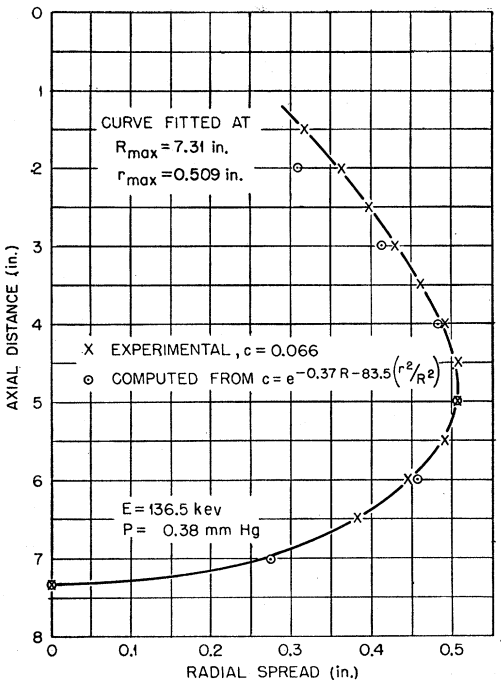

FIG. 15. Curve-fitting of the function $C+\exp(-AR-Br^2/R^2)$ for A^+ ions in argon gas.

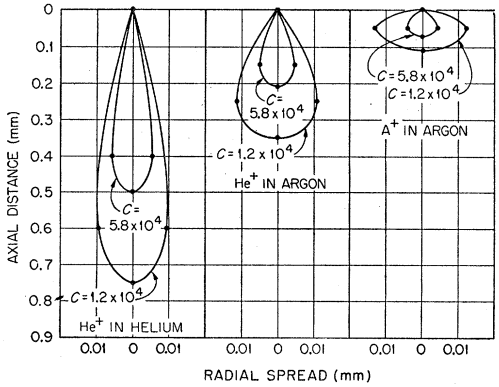

FIG. 16. Ionization density contours at 1-atmosphere pressure.

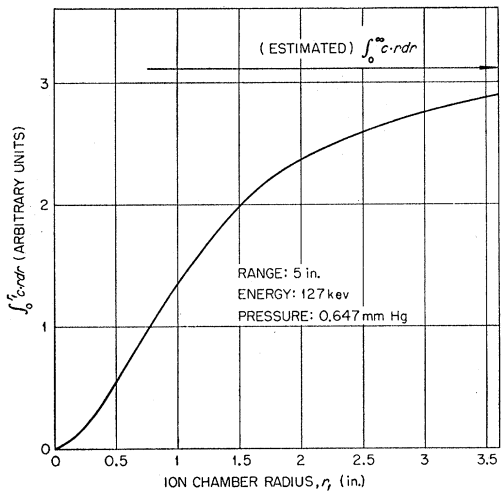

FIG. 17. Ion chamber current *vs* ion chamber radius.

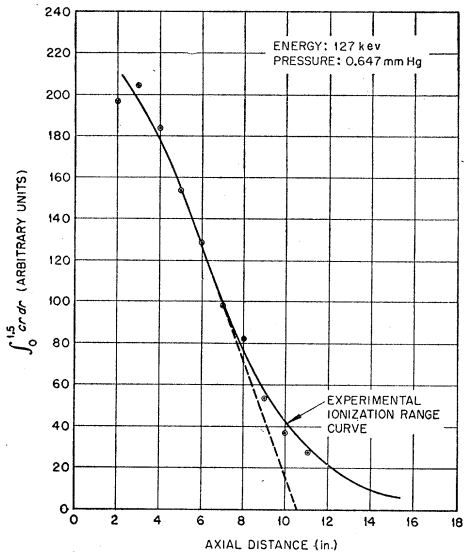

FIG. 18. Comparison of ionization range curve as computed and as measured directly. The circled points correspond to values of $\int_0^{1.5} C \cdot r\, dr$.

contours as computed for $P=1$ atmos are shown in Fig. 16.

From a knowledge of the distribution of ionization in a plane normal to the beam axis, it is possible to predict the behavior of a thin parallel plate ionization chamber placed in the beam. Values of the function $\int_0^{r_1} C \cdot r\, dr$ evaluated in the plane $R=R_1$ are proportional to the ionization current which would be produced by an ionization chamber of radius r_1 placed at a distance R_1 from the source of the beam. A typical plot of the function $\int_0^{r_1} C \cdot r\, dr$ is plotted against r_1 in Fig. 17, where the ionization distribution is that produced by 127-kev argon ions stopping in argon gas at 0.647-mm Hg pressure, at a distance R of 5 inches. It is evident that in order to stop essentially all of the ions crossing the plane at $R=5$ inches that an ionization chamber considerably larger in diameter than 6 inches is required under these conditions, and that the three inch diameter ionization chamber used in the experiments described in Part III of this paper would fail to detect approximately $\frac{1}{3}$ of the ions capable of reaching the plane at $R=5$ inches. By computing values of the function $\int_0^{1.5''} C \cdot r\, dr$ for a series of values of R and plotting these integrals against R, the resulting curve should duplicate the ionization range curve at the same pressure as obtained in Part III of this paper. The circled points shown plotted on Fig. 18 were obtained by graphical integration of ionization density data, while the solid curve is that obtained with the equipment described in Part III. The agreement is seen to be within 2 percent. Similarly, if values of the integral $\int_0^\infty C \cdot r\, dr$ are plotted against R, the resulting range curve should correspond to that obtained with a hypothetical ionization chamber of infinite diameter, and extrapolation of this range curve to the zero current should lead to the range value R_E defined in Part III. In actual practice it is difficult to obtain accurate values of R_E in this way because of the large uncertainty in evaluating the integrals over the "tails" of the function $C \cdot r$ extending beyond the maximum radius $r=3.5$ inches, as can be seen by inspection of Fig. 17. For the set of data from which Fig. 17 was drawn, the agreement of the values of R_E as obtained by extrapolating R_A values against $1/P$ and as obtained by plotting values of $\int_0^\infty C \cdot r\, dr$ against R agreed to well within the limits imposed by the uncertainty in the integration of the "tails."

It is evident that for each energy and each incident ion-stopping gas combination one has a distinct set of ionization density contours. Since necessarily the number of such sets that can be reproduced here is limited, interested parties are invited to contact the authors directly for further detail.

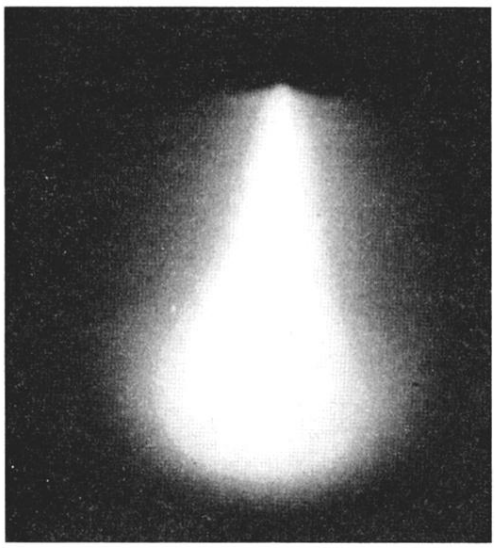

FIG. 12. Photograph of the luminescence produced by the beam: He^+ ions in argon. Energy = 136 kev.